Modular High Power Density Integrated Motor with Fault Tolerance

xxxxxxx

***Abstract*— Vehicles using electric drive trains are gaining high importance since the beginning of the last decade. Special areas were later drives will be used have high requirements in terms of safety and fault tolerance especially if the vehicle is traveling via air. This paper presents a modular integrated axial flux permanent magnet machine which is tackling the challenges in the terms of fault tolerance and power density regarding to volume and weight. The proposed drive uses several GaN based power semiconductor inverters and a field-oriented control.**

***Index Terms*— Aerospace safety, Closed loop control, Fault tolerance, Gallium nitride, High power density motor, Motor drives, Integrated design, Unmanned aerial vehicles.**

I. Introduction

Electrically propelled vehicles are gaining importance particular in the area of passenger and payload transportation. Latter task is usually carried out by Unmanned Aerial Vehicles (UAV) which start to emerge rapidly. Especially in the monitoring of natural hazards [1] and agriculture [2], [3] recent scientific work is ramped up. Every of these mentioned applications benefit of longer operation time as well as being able to carry higher payloads. It is therefore vital for the drive system to have a low empty weight as well as a high efficiency of the motor itself and its power electronics. Additionally some vehicles like UAVs need to fulfil, depending on the region, several safety standards. One of these later is to have redundancy in the motor drive in order to be fault tolerant. In this case even major faults do not lead to a crash of the UAV. Similar requirements for fault tolerance are also postulated for drive systems in the automotive area. One strategy to achieve a certain fault tolerance can be in the inverter design [4] or by the use of a modular drive structure [5] [6]. In order to achieve the, also rather conflictive goals, a modular integrated axial flux permanent magnet machine is proposed. Axial flux permanent machines (AFPM) have been shown to yield in higher torque and power density in several cases [7] and motor sizes [8] compared to radial flux machines. [9] [10]

The proposed motor consist out of individual phases which are supplied by individual inverters in order to reach a high failure tolerance to even destructive errors. To still be able to reach a high power density, special care has been taken in the thermal design procedure like in [11] as well as the utilization of wide-band gap semiconductors [12] [13] [14]. In addition an integrated design is chosen as this will result in higher power density as well as a lower sensitivity to failures due to a more enclosed design [15] [16] [17] [18] [19]. In chapter II a brief system overview will be given showing the main components and design concepts. Chapter III is illustrating the control algorithm and architecture. The last chapter is giving a sum up of the whole paper.

II. System Overview

To achieve a high power density as well as a high system reliability, the inverters as well as the motor are combined in one structure. This step has two advantages, once everything can be enclosed and thus make it less prone to environmental effects as well as serve as a heatsink for the inverters. In Fig. 1 one can see a schematically view of the mechanical system. In the case for a UAV the propeller used to create the lift force is generating an airflow around the structure which is cooling down the inverters inside. At a higher trust more losses are generated but also a higher airflow velocity which in turn removes even more heat.

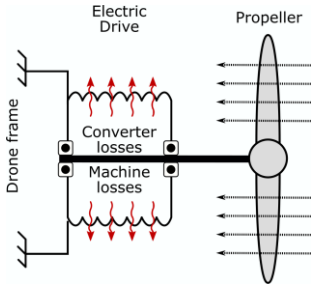

Fig. 1: Mechanical structure

One of the major goals for the electrical drive system in a vehicle is redundancy. If an UAV with four motors would be used, a malfunction of one motor will result in an uncontrollable behaviour of the whole system. It is therefore important to either increase the number of individual motors or make them on their own redundant. Our proposal is therefore to instead of having only three inverters and three phases a multisystem approach is used. By having four independent systems a critical error in one of the later will result only in a reduction of the maximum achievable thrust.

A. Electric Motor

As radial motors show a lower torque for the same volume, an axial flux permanent machine (AFPM) is chosen. The stator can be seen in Fig. 2. It consists of 12 windings resulting in a maximum of 4 independent systems. Several considerations have been done in order to reduce the losses of the motor and make it less prone to failures.

Fig. 2: Stator of the AFPM

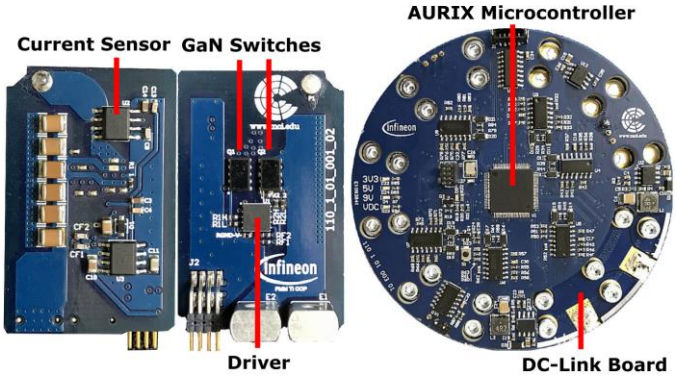

Fig. 4: Realised electronics (a) Bottom side of inverter PCB. The DC-link capacitors can be seen on the left, the current sensor on the top and an LDO on the bottom. (b) Top side of inverter PCB with the two GaN switches in the middle and the driver below. (c) Top side control PCB with mounted DC-Link PCB and inverter PCBs via hexagon socket screws.

B. Power converter structure

The drive is composed by 4 electrically isolated systems each connected to an inverter with common DC-link. In Fig. 3 the proposed structure is illustrated. In total a minimum of 12 half-bridges are needed in order to operate the individual systems of the AFPM. Furthermore a controller board and DC-Link board are needed. The controller board consists of measurement electronics and an Aurix microcontroller which is calculating and generating the PWM signal needed for the inverters. Between the controller board and the inverters is the so called DC-Link board which is responsible for distributing the supply voltage to the individual inverters, where GaN switches, driver and current sensor are implemented.

In Fig. 4 the realized hardware is depicted. In Fig. 4 (a) the bottom side of the inverter is shown. It consists mainly out of DC-Link capacitors as well as the current sensor and a 5V voltage regulator. On the top side, see Fig. 4 (b) the GaN switches are mounted as well as the gate driver circuit. The pin headers are used to transmit the PWM signals as well as the logic supply voltage to the inverter from the controller board. Additionally the measured current is fed back to the controller board via the pin headers. At the bottom right, two special connectors are shown, used to connect the inverters to the DC-Link board, with hexagon socket screws. On Fig. 4 (c) one can see the screws in the DC-Link board which is below the controller board. The inverters are mounted on the outer radius of the controller board in an angle of 30° apart. The pin headers cannot be seen as they are connected on the bottom side.

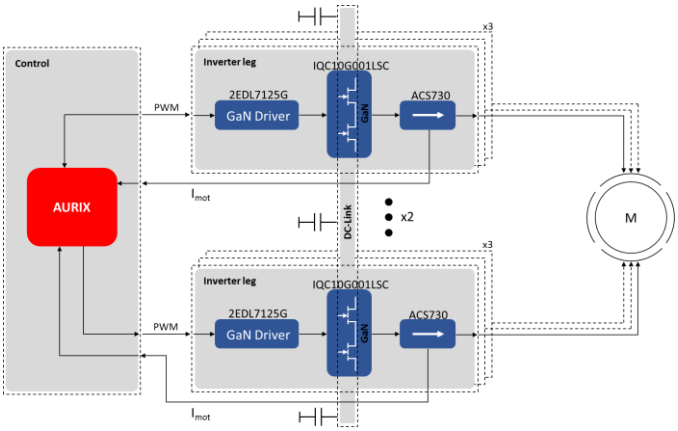

Fig. 3: Proposed electronics design

C. Complete System

The complete system is depicted in 5. The assembly is as follows: the rotor and bearings are mounted together with the stator in between on the shaft. Then the stator can be fixed to the aluminium frame. In the next step the inverters are connected by soldering the cables from the stator. Afterwards the top lid can be closed providing the support for the second bearing. The next step is to put a thermal interface material onto the aluminium where the inverters are mounted. The inverters are additionally pressed with a spring, not visible in the pictures, to the aluminium wall in order to achieve a good thermal connection to the structure.

When the inverters are mounted, the DC-Link board can be screwed onto the frame. Now the inverters can be connected with the hexagonal screws in order to assure a proper alignment for the pin header. At last the controller board is mounted by pressing the board with the aligned pin header sockets onto the inverters. Afterwards also the bottom lid can be closed.

The specifications of the total system are summarized in Table I and II.

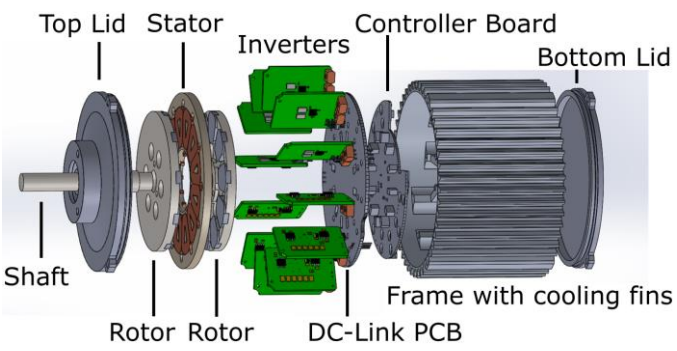

Fig. 5: Explosion drawing of the complete system

TABLE I
PERFORMANCES OF THE ELECTRIC MACHINE

PARAMETER	Value
Rotor pole	10
Number of coils	12
Mechanical speed	15000 rpm
Rated Torque	0.7 Nm
Rated current	15 Arms
Fundamental frequency	1250 Hz
Efficiency	95%
Outer Diameter	78 mm
Axial length	17 mm

TABLE II
POWER DENSITIES OF THE ELECTRIC DRIVE

Item	WEIGHT	Power densities
Electric Motor	410 g	2.43 kW/kg
Power converter	152 g	9.47 kVA/kg
Frame and covers	560 g	
Bearings, shaft …	122 g	
Overall	1.24 kg, 0.698 *l*	0.83 kW/kg, 1.43 kW/*l*

III. CLOSED LOOP CONTROL ALGORITHMIC

Different loads are applied to a UAV motor depending on various circumstances. This can be a change in flight speed but also approaching or lifting off the ground. A closed loop control is therefore vital for a high efficient operation. A principle diagram of the realized control algorithm, is shown in Fig. 7. A 20 kHz trigger activates the control algorithm. First it is checked if a hall sensor trigger has occurred therefore a new speed can be calculated out of which the new rotor position is estimated. Then the ADC conversion of the phase currents is fetched from the result register, which is updated with 200kHz, in order to perform the Clark/Park transformation for the d/q coordinate system. The resulting dq-currents are then fed into the PI control with feed forward. Out of its result the inverse Park transform can be calculated which can be used to yield in the angle and magnitude information needed to realise a Space Vector Pulse Width Modulation (SVPWM) which is calculating the on-times for the half-bridges switching at 200kHz.

In Fig. 6 the phase currents of one system controlled to a reference peak current of 2A are shown. It can be noticed that even at this low speed the current waveform is sinusoidal and controlled to the reference value of 2A. To reach higher speeds the angle generation has to be of main focus as well as implementing a sensorless control scheme.

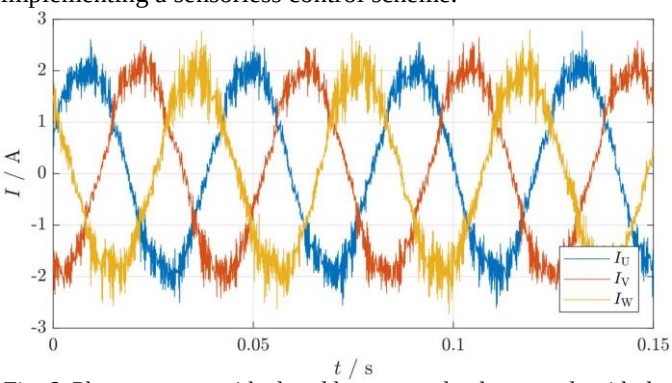

Fig. 6: Phase currents with closed loop control at low speeds with the peak current reference set to 2A.

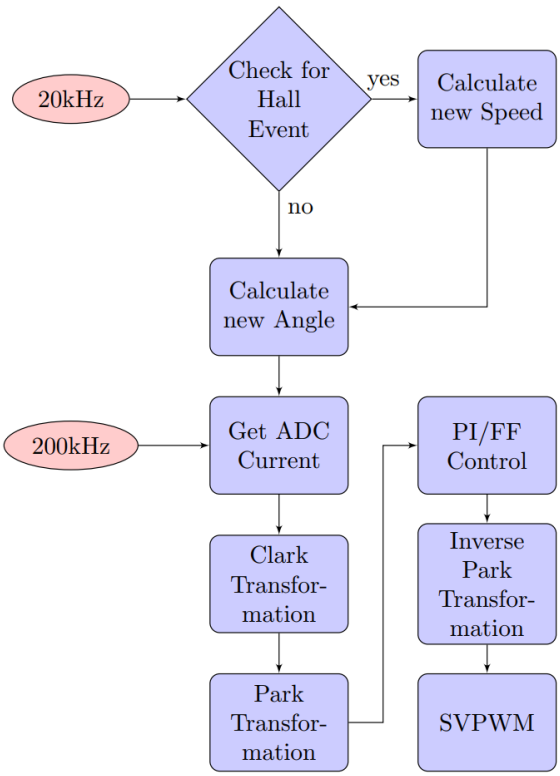

Fig. 7: Control algorithm diagram

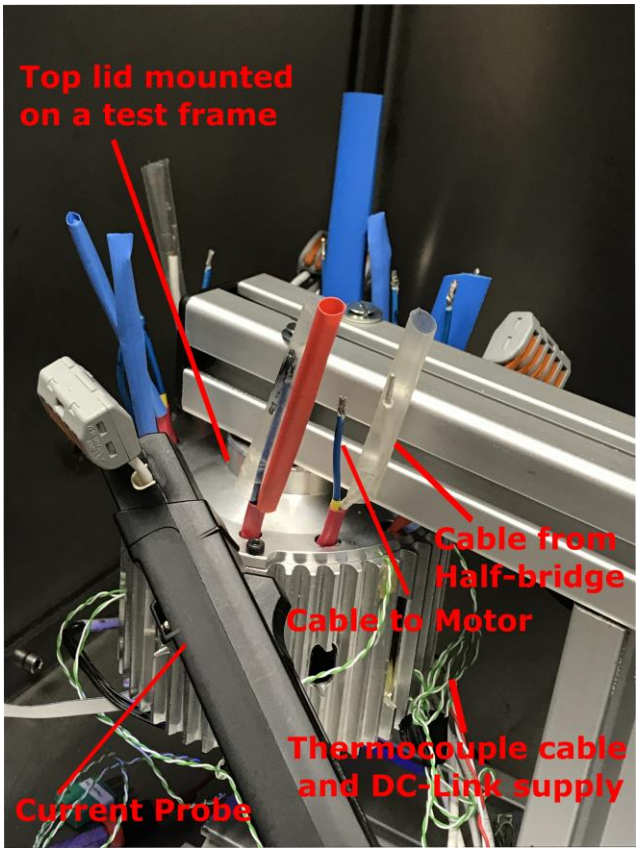

Fig. 8: Testing installation for the complete system. The cables from the half-bridges to the stator windings are lead out in order to fit a current probe.

Fig. 8 shows the testing installation used to carry out all measurements. The drive is mounted on the test frame in order for the shaft to be oriented vertical. The cables from the half-bridge boards to the individual motor phases are lead out in order to be able to measure the current into the stator windings with a current probe. Additionally to the current measurement, several thermocouples are places around various positions to measure the temperature.

IV. Conclusion

This paper has presented a high power density integrated drive. Especially in the field of UAVs high power density and reliability are an integral part of the complete system. With the shown drive system these challenges are addressed. In combination with the right control scheme and robust implementation, the drive can be used additionally in industrial application were high speed motors are needed. The enclosed design allows even the operation in dusty and potentially humid environments. Future work will concentrate on improving the main characteristics of the motor even further as well as realizing a fault tolerant algorithm which can react to different failure scenarios.

References

[1] D. Giordan, A. Manconi, F. Remondino and F. Nex, "Use of unmanned aerial vehicles in monitoring application and management of natural hazards," *Geomatics, Natural Hazards and Risk,* pp. 1-4, 02 May 2017.

[2] Y. Guijun, L. Jiangang, Z. Chunjiang and a. et., "Unmanned Aerial Vehicle Remote Sensing for Field-Based Crop Phenotyping: Current Status and Perspectives," *Frontiers in Plant Science,* 2017.

[3] Y. Shi, J. Thomasson, S. Murray, N. Pugh, W. Rooney and a. et, "Unmanned Aerial Vehicles for High-Throughput Phenotyping and Agronomic Research," *PLOS ONE,* 2016.

[4] B. A. Welchko, T. A. Lipo, T. M. Jahns and S. E. Schulz, "Fault Tolerant Three-phase AC Motor Drive Topologies; A Comparison of Features, Cost, and Limitations," *IEEE Transactions on Power Electronics,* pp. 1108-1116, July 2004.

[5] M. Uğur and O. Keysan, "Design of a GaN Based Integrated Modular Motor Drive," *XIII International Conference on Electrical Machines (ICEM),* September 2018.

[6] Z. Wenxiang, C. Ming, H. Wei and J. Hongyun, "A Redundant Flux-Switching Permanent Magnet Motor Drive for Fault-Tolerant Applications," *IEEE Vehicle Power and Propulsion Conference,* September 2008.

[7] F. Caricchi, F. Crescimbini and O. Honorati, "Modular Axial-Flux Permanent-Magnet Motor for Ship Propulsion Drives," *IEEE Transactions on Energy Conversion,* pp. pp. 673-679, September 1999.

[8] A. Cavagnino, M. Lazzari, F. Profumo and A. Tenconi, "A Comparison Between the Axial Flux and the Radial Flux Structures for PM Synchronous Motors," *IEEE Transactions on Industry Applications,* pp. 1517-1524, Nov.-Dec. 2002.

[9] M. Aydin, S. Huang and T. A. Lipo, "Axial Flux Permanent Magnet Disc Machines: A Review," *WEMPEC,* January 2004.

[10] D. J. Patterson, J. L. Colton, B. Mularcik, B. J. Kennedy, S. Camilleri and R. Rohoza, "A Comparison of Radial and Axial Flux Structures in Electrical Machines," *IEEE International Electric Machines and Drives Conference,* May 2009.

[11] L. Woongkul and S. Bulent, "Thermal Analysis of Lateral GaN HEMT Devices for High Power Density Integrated Motor Drives Considering the Effect of PCB Layout and Parasitic Parameters," *IEEE Transportation Electrification Conference and Expo (ITEC),* June 2018.

[12] A. Morya, M. Moosavi, M. C. Gardner and H. A. Toliyat, "Applications of Wide Bandgap (WBG) Devices in AC Electric Drives: A Technology Status Review," *IEEE International Electric Machines and Drives Conference (IEMDC),* May 2017.

[13] W. Jiyao, L. Ye and H. Yehui, "Evaluation and Design for an Integrated Modular Motor Drive (IMMD) with GaN devices," *IEEE Energy Conversion Congress and Exposition,* September 2013.

[14] W. Jiyao, L. Ye and H. Yehui, "Integrated Modular Motor Drive Design with GaN Power FETs," *IEEE Transactions on Industry Applications,* June 2015.

[15] A. Robert, V. Gaurang, L. C. Giovanni, C. Thomas, L. Simon, J. Mark, G. Chris and M. Barrie, "Integrated motor drives: state of the art and future trends," *IET Electric Power Applications,* pp. pp. 757-771, 2016.

[16] N. Brown, T. Jahns and R. Lorenz, "Power Converter Design for an Integrated Modular Motor Drive," *IEEE Industry Applications Annual Meeting,* pp. 1322-1328, 2007.

[17] A. M. EL-Refaie, "Integrated Electrical Machines and Drives: An Overview," *IEEE International Electric Machines & Drives Conference,* May 2015.

[18] T. M. Jahns and D. Hang, "The Past, Present, and Future of Power Electronics Integration Technology in Motor Drives," *CPSS TRANSACTIONS ON POWER ELECTRONICS AND APPLICATIONS,* September 2017.

[19] J. Wolmarans, M. Gerber, H. Polinder, S. de Haan, J. Ferreira and D. Clarenbach, "A 50kW Integrated Fault Tolerant Permanent Magnet Machine and Motor Drive," *IEEE Power Electronics Specialists Conference,* June 2008.